REVIEW ARTICLE

Plasmonic light trapping in thin-film Si solar cells

P Spinelli[1], **V E Ferry**[2], **J van de Groep**[1], **M van Lare**[1], **M A Verschuuren**[3], **R E I Schropp**[4], **H A Atwater**[2] and **A Polman**[1]

[1] Center for Nanophotonics, FOM Institute AMOLF, Science Park 104, 1098 XG Amsterdam, The Netherlands
[2] Thomas J Watson Laboratories of Applied Physics, California Institute of Technology, Pasadena, CA 91125, USA
[3] Philips Research Laboratories, High Tech Campus 4, 5656 AE Eindhoven, The Netherlands
[4] Debye Institute for Nanomaterials Science, Section Nanophotonics, Utrecht University, PO Box 80.000, 3508 TA Utrecht, The Netherlands

E-mail: polman@amolf.nl

Abstract
Plasmonic nanostructures have been recently investigated as a possible way to improve absorption of light in solar cells. The strong interaction of small metal nanostructures with light allows control over the propagation of light at the nanoscale and thus the design of ultrathin solar cells in which light is trapped in the active layer and efficiently absorbed. In this paper we review some of our recent work in the field of plasmonics for improved solar cells. We have investigated two possible ways of integrating metal nanoparticles in a solar cell. First, a layer of Ag nanoparticles that improves the standard antireflection coating used for crystalline and amorphous silicon solar cells has been designed and fabricated. Second, regular and random arrays of metal nanostructures have been designed to couple light in waveguide modes of thin semiconductor layers. Using a large-scale, relative inexpensive nano-imprint technique, we have designed a back-contact light trapping surface for a-Si:H solar cells which show enhanced efficiency over standard randomly textured cells.

Keywords: plasmonics, solar cells, light trapping, thin-film

(Some figures in this article are in colour only in the electronic version)

1. Introduction

Photovoltaics are a promising technology for generating electrical power from the Sun on a large scale, with the potential to meet a significant part of the increasing worldwide energy demand. Growth in installed solar power has been very large over the last few years, as new technologies have both improved the cell efficiency and reduced production costs. However, so far the price of solar-generated electrical power has remained above the price of power generated by conventional sources of energy. Reducing the overall cost per watt is thus one of the major challenges in solar cell research. The price of an installed solar cell includes both material and processing costs as well as system costs. Materials and processing represent a large fraction of the expense. For example, in bulk crystalline silicon solar cells, material costs account for 40% of the final module price. Recently, thin-film solar cell technology has emerged as a way to reduce the material costs. Due to the reduced material volume of thin-film devices, semiconductors containing scarce elements such as CdTe and $CuInGaSe_2$ have entered the market to compete with bulk crystalline Si and thin-film Si solar cells. The combination of low manufacturing costs and reasonable efficiencies make thin-film photovoltaics an attractive option for reducing the total cost per watt of solar power. Additionally, for bulk recombination-dominated semiconductors, thin-film
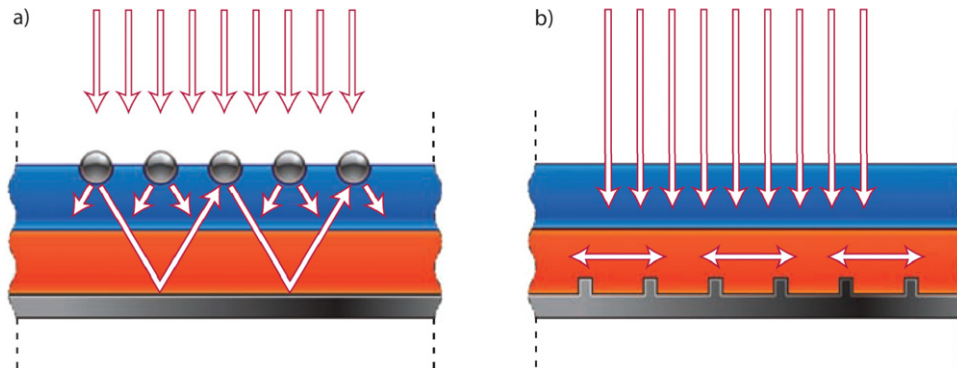
Figure 1. Two possible concepts of plasmonic nanostructure integration for solar cells. (a) Light trapping by enhanced forward scattering from metal nanoparticles placed on top of the solar cell, and by angular redistribution of the scattered light. (b) Light trapping by light coupling into photonic modes of the semiconductor due to corrugation in the metal back surface. Figures reproduced with permission: ©Amolf/Tremani/Nature Publishing Group (2010).

solar cells also present the advantage of better carrier collection and reduced bulk recombination, both factors improving the solar cell efficiency.

As the thickness of the absorbing semiconductor is reduced, however, the absorption naturally decreases at energies close to the electronic bandgap of the semiconductor. This is particularly a problem for thin-film Si devices. Devices based on crystalline or microcrystalline Si have poor absorption near the bandgap, where the absorption length is $>300 \mu$m. Light trapping schemes are thus needed to enhance light absorption. In conventional thick Si solar cells, light trapping is typically achieved using a micron-sized pyramidal surface texture that causes scattering of light into the solar cell over a large angular range, thereby enhancing the effective path length in the cell [1–3]. Such geometries are not suitable for thin-film cells, as the cell thickness is smaller than the texturing size and the greater surface area increases minority carrier recombination at the surface. Furthermore, texturing is not applicable to non-single-crystal cells.

Recently, metallic nanostructures supporting surface plasmons have been proposed as an alternative method to achieve light trapping in thin-film solar cells [4, 5]. These subwavelength nanostructures strongly interact with sunlight and, if properly engineered within the solar cell geometry, can concentrate and fold light into thin semiconductor layers, thereby enhancing the absorption. Two different concepts of plasmonic nanostructure integration for solar cells comprise most of the investigations to date. In the first scheme, metal nanoparticles placed on the top of the solar cell (figure 1(a)) scatter incident sunlight into the solar cell. These particles preferentially scatter light into the high-index substrate, leading to enhanced coupling to the underlying semiconductor and thus reduced reflectance over a broad spectral range. Besides this antireflection (AR) effect, the angular redistribution of the scattered light also contributes to light trapping by increasing the optical path length inside the cell. If the semiconductor is instead a thin film, an array of metal nanoparticles placed on top can additionally couple the light into guided modes in the semiconductor slab. In the second scheme (figure 1(b)), the metal back contact of a thin-film solar cell is patterned directly, without introducing

any extra metal features. The blue light is absorbed as in a standard solar cell, while the red light couples from the nanostructures into the guided modes of the semiconductor, as well as to surface-plasmon-polariton (SPP) modes that may be supported at the back metal/semiconductor interface. Light in the propagating waveguide mode is then absorbed in the plane of the semiconductor, while carrier collection occurs out of plane, allowing for a reduction in overall thickness. For any given waveguide mode, some fraction will be absorbed in the semiconductor and some lost to the cladding layers [6, 7].

In this paper we review some recent developments in the use of plasmonic nanostructures to improve solar cells, both by means of the improved AR effect and by coupling to waveguide modes. We make use of both experimental and theoretical techniques for studying light trapping. In section 2, a systematic study of the plasmon-mediated light coupling into a substrate by metal nanostructures placed at the front of the solar cell is presented. We investigate the effect of particle shape, size and array pitch on the coupling of light, using both simulation and experiments. Total reflectance spectroscopy carried out on a thick c-Si solar cell shows that optimized plasmonic AR coatings can be better than standard planar dielectric coatings. The second part of this paper analyzes the coupling of light to guided optical modes in a thin semiconductor layer. A silicon-on-insulator wafer with a 200 nm c-Si region is used as a model system for solar cells to investigate the mechanism of light coupling to waveguide modes in ultrathin optically active layers. The coupling to waveguide modes is studied theoretically, using a transfer matrix method, and experimentally, using photoluminescence of Er^{3+} ions in the waveguide as a probe of trapped light intensity. In the third section, we demonstrate integration of plasmonic nanostructures into a full solar cell device to enhance efficiency and explore nanostructure arrangements on the back contact of an a-Si:H solar cell using both experiment and simulation. The patterns are fabricated using an inexpensive and scalable nano-imprint process and show enhanced efficiency over randomly textured reference cells. Coupling to waveguide modes is clearly observed in the sharp features in the measured and simulated external quantum
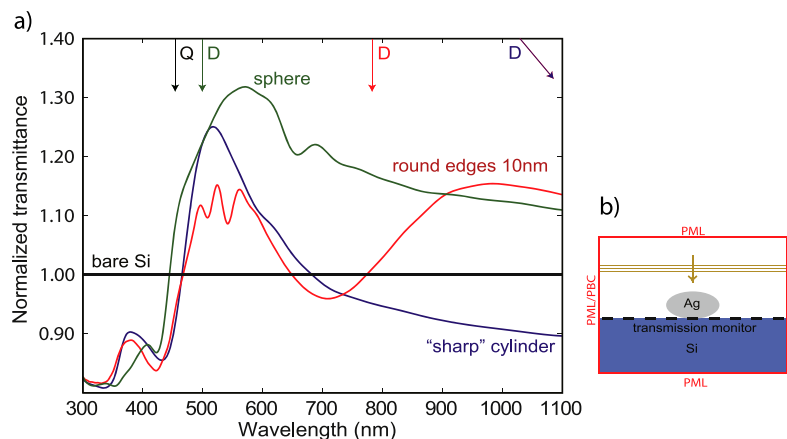
Figure 2. (a) Transmittance spectrum for single Ag nanoparticles of different shapes on top of an Si substrate, calculated using FDTD. Data are normalized to the transmittance for a bare Si substrate. The transmission is enhanced for wavelengths above the Ag particle plasmon resonance (arrows below the top axis) and suppressed for wavelengths below (Fano effect). The strong redshift of the plasmon resonance for particles of cylindrical shape leads to a broadening of the Fano reduction, thus making spherical particles preferable for light coupling. (b) Schematic of the FDTD simulation geometry. Figures reproduced with permission: (a) ©OSA (2011), (b) ©ACS (2011).

efficiency (EQE) spectra and confirmed by angle-resolved photocurrent spectroscopy.

2. Plasmonic antireflection coatings

Standard dielectric interference coatings are usually optimized for a particular wavelength and incident angle and thus reduce reflectance over a relatively narrow bandwidth. Recently, metal nanoparticles deposited onto a substrate have been studied to increase the coupling of light into a substrate. The resonant scattering due to plasmon resonances in the metallic particles leads to reduced reflection over a broad spectral range [8–10]. Many experimental papers have studied this AR effect of random nanoparticle configurations, with limited control over the particle geometry [11–17]. Recently, we have performed a systematic experimental and numerical study of the light coupling by regular arrays of metal nanoparticles [18, 19].

We use finite-difference time domain (FDTD) simulations to study the enhanced transmission of light into a thick c-Si substrate by arrays of silver nanoparticles placed on its top surface. The simulation configuration used for this study is shown in figure 2(b). A silver nanoparticle is placed on the top of a semi-infinite c-Si substrate and a broadband (wavelength 300–1100 nm) plane-wave pulse is incident on the particle from the top. A frequency domain monitor placed 1 nm below the c-Si surface directly measures the total power transmitted into the substrate. Periodic boundary conditions (PBC) are used to simulate an array configuration, whereas perfectly matched layers (PML) are used for a single-particle configuration. Figure 2(a) shows the transmission spectra normalized to the transmission of a bare c-Si substrate for three different particle shapes: a sphere (green), a cylinder with a 10 nm round edge (red) and a cylinder with a sharp edge (blue). The arrows in the top part of the graph indicate the position of the dipolar resonance (colored arrows) and quadrupolar resonance (black arrow) for each of the particle shapes. The dipolar resonance is strongly redshifted when the

shape changes from a sphere to a cylinder, due to the stronger near-field coupling to the high-index substrate for a cylinder with respect to a sphere [18, 20]. The quadrupolar resonance, on the other hand, does not shift when the particle shape is changed.

The graph in figure 2(a) shows that in the spectral range with wavelengths longer than the resonance the transmission is enhanced by the presence of the nanoparticle. The mechanism behind this effect is the preferential scattering of light at the particle resonance into the high-index substrate, due to the higher density of states in the substrate [8, 21, 22]. Enhancement in light transmission is seen for both the dipolar and quadrupolar modes for the sphere and rounded cylinder in figure 2(a); for the sharp cylinder the dipole resonance is outside the range of the graph. In contrast, a clear reduction of the coupled power occurs with wavelengths shorter than each resonance. This reduction occurs due to a Fano effect, i.e. a destructive interference between scattered and incident light occurring at wavelengths below resonance [23–25].

The redshift of the plasmon resonance that occurs when the shape changes from a sphere to a cylinder leads to a broadening of the Fano reduction for wavelengths shorter than the resonance. For a sharp cylinder, with the dipolar resonance longer than 1100 nm, this reduction in transmittance is quite strong. Figure 2(a) thus clearly shows that a spherical shape is preferable for enhancing light coupling into a c-Si substrate.

An optimization of the size and array parameters for spheroidal particles can be found in [19]. In that paper, transmission spectra for different geometries were simulated in the same way as figure 2(a) and an average transmittance is calculated by weighting over the standard AM1.5 solar spectrum. The array of nanoparticles is placed on top of an Si_3N_4 spacer layer, which acts as an interference AR coating and provides a blueshift of the plasmon resonance with respect to the case of particles on a bare Si substrate [9, 26], thus reducing the Fano reduction at short wavelengths. The optimal configuration is found for 200 nm diameter, 125 nm high Ag
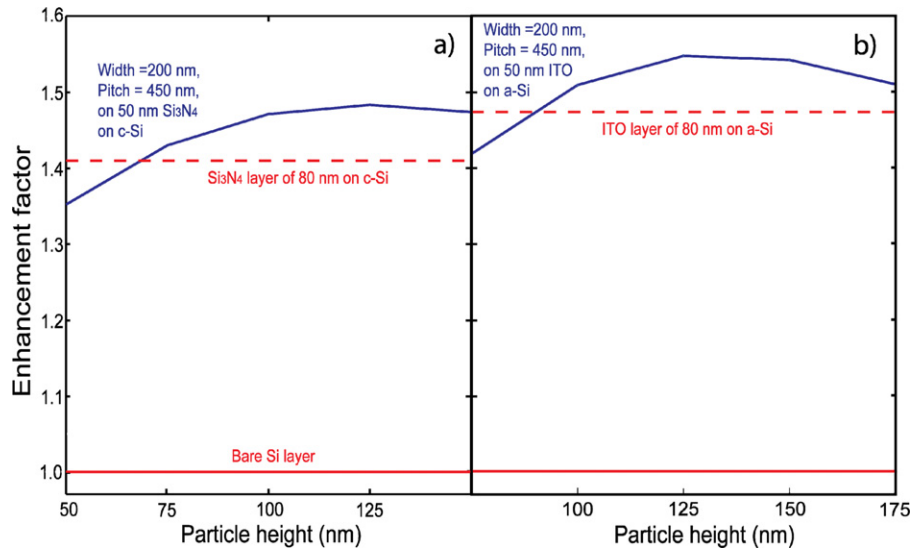
Figure 3. Transmission enhancement for Ag particle arrays on c-Si with a 50 nm thick Si_3N_4 spacer layer (a) and on a-Si with a 50 nm thick ITO spacer layer (b), integrated over the AM1.5 solar spectrum and relative to a bare substrate. Data are shown for different particle heights. The best geometries show 8% higher transmittance with respect to a standard 80 nm thick Si_3N_4 AR coating for a c-Si substrate and 9% higher transmittance with respect to a standard 80 nm thick ITO AR coating for an a-Si substrate (dashed red lines). Figure (a) reproduced with permission: ©ACS (2011).
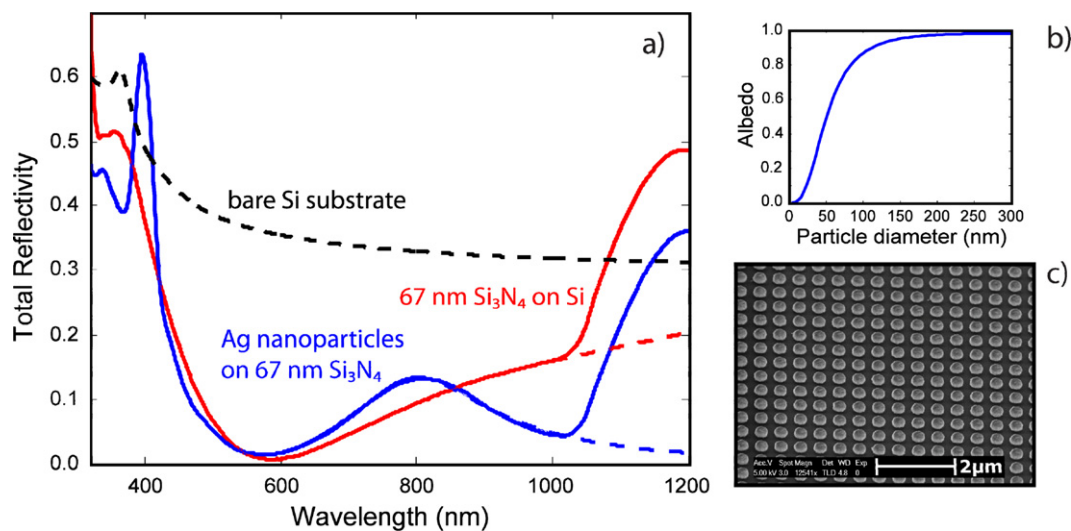

Figure 4. (a) Measured total reflection spectrum from a 300 μm crystalline Si cell coated with 67 nm Si_3N_4 (red) and the same sample with an optimized Ag particle array on top (blue). The particles reduce the reflection for wavelengths above 800 nm, improving the coupling of light into the Si substrate. The dashed lines are extrapolated data representing the reflection from a semi-infinite substrate. The calculated reflectance of a semi-infinite Si substrate is shown for reference (dashed black line). (b) Calculated albedo of a silver nanoparticle in air as a function of particle diameter. (c) An SEM image of the optimal Ag nanoparticle arrays. Figures reproduced with permission: ©ACS (2011).

nanoparticles, with an array pitch of 450 nm, on top of a 50 nm thick Si_3N_4 spacer layer on a semi-infinite c-Si substrate. Figure 3 shows the average transmittance for arrays of Ag nanoparticles with different heights on top of an Si_3N_4 layer on a semi-infinite crystalline silicon substrate (figure 3(a)) and on top of an ITO spacer layer on a semi-infinite a-Si:H substrate (figure 3(b)). In both cases, the plasmonic AR coating combined with the standard interference coating yields a higher transmittance than the standard interference coating alone. In the case of a c-Si substrate, the overall transmittance

is improved by 8% with respect to a standard AR coating, while for a plasmonic coating on an a-Si:H substrate the transmittance is improved by 9%.

An experimental proof that optimized plasmonic coatings are better than a standard AR coating is shown in figure 4 [19]. A 2 × 2 mm² wide array of Ag nanoparticles (180 nm diameter, 130 nm high with an array pitch of 450 nm) was fabricated by means of electron-beam lithography (EBL) on top of a 67 nm thick Si_3N_4 layer on an Si(100) substrate. Figure 4(c) shows a scanning electron microscopy (SEM)

image of such an array (metal surface coverage 30%). The measured total reflectance from the bare interference coating (red) and for the optimized plasmonic coating (blue) is shown in figure 4(a). The reflection spectrum for a c-Si substrate coated with 67 nm of Si_3N_4 shows the typical trend for an interference AR coating, yielding a minimum in reflection around 600 nm. Adding the particle array yields a broadband reduction in total reflection at wavelengths longer than 850 nm and does not drastically affect the light coupling for shorter wavelengths. The sharp reflection increase at wavelengths longer than 1050 nm in both curves is due to light that is reflected from the back contact that is not absorbed in the c-Si substrate. Indeed, the absorption length of c-Si at 1050 nm equals 600 μm, i.e. twice the cell thickness. The dashed lines in figure 4(a) are extrapolations of the data, representing the reflectivity of a semi-infinite substrate sample, made using a linear fit for the bare substrate (red) and a Lorentzian fit for the substrate with particles (blue) on the dataset in the 600–1000 nm spectral range. The calculated reflectance of a bare Si substrate is shown as a reference (dashed black line).

Measuring reflectance does not confirm whether the absorption occurs in the c-Si layer or in the Ag nanoparticles, but we address this question with simulation. Figure 4(b) shows the calculated albedo of a silver nanoparticle in air as a function of particle diameter. For particles of 180 nm diameter, as used in the experiment, the albedo amounts to 97%, meaning that only 3% of the light is absorbed by ohmic dissipation in the Ag nanoparticles. For particles on a higher-index substrate, the albedo is even higher, as the scattering is enhanced due to the higher density of states in the substrate. It is therefore reasonable to conclude from figure 4 that the absorption in the c-Si layer is enhanced by the presence of the metal nanoparticle array on top. An estimation of the absorption enhancement in the active layer can be made from the reflectivity data in figure 4(a). The plasmonic coating was found to enhance light absorption by more than 20% with respect to a standard AR coating for wavelengths close to the Si bandgap wavelength, i.e. in the region where Si poorly absorbs light (for a broader discussion see [19]).

3. Light coupling to waveguide modes in a thin c-Si layer

Besides the AR effect, metal nanoparticle arrays provide an efficient light trapping scheme for thin-film solar cells, for which standard light trapping methods such as pyramidal surface texturing cannot be used. It is well known that ultrathin dielectric layers support a discrete and limited set of guided optical modes [27]. Light that is coupled into these modes is efficiently trapped inside the slab, resulting in a drastic increase of optical path length. Plasmonic nanoparticle arrays printed on top of a thin-film solar cell can couple light to the waveguide modes in the optically active layer, thus providing an efficient light trapping mechanism. The interaction between metal nanoparticle arrays and waveguides was first studied by Stuart and Hall, who observed a strong influence on the inter-particle interaction as a result of the presence of waveguide modes in the substrate [28].

Here, a silicon-on-insulator wafer with a 200 nm Si waveguide is used as a model system for a solar cell to investigate the mechanism of light coupling to waveguide modes in ultrathin optically active layers. While most thin-film Si solar cells are not c-Si but either microcrystalline or a-Si:H, this platform serves as a model system since it shows the effects of light trapping very strongly. The waveguide modes supported in the c-Si region of the SOI wafer are calculated by using the transfer matrix method from [29]. By applying the boundary conditions for the field at each interface, the field distribution as well as the complex in-plane wavevector $k_z = \beta + i\kappa$ of all modes supported by any arbitrary multilayer waveguide are calculated.

The inset of figure 5(a) shows a schematic of the layer structure used in the calculations. A thin dielectric spacer layer is introduced on top of the waveguide. In figure 5(b) the mode profiles as a function of depth *y* are shown for all the TE modes (electric field in plane with the waveguide), together with the in-plane wavevector. The gray vertical dashed lines represent the interfaces between the different layers of the structure. Figure 5(b) shows that all the modes are mainly localized in the c-Si waveguide region. Furthermore, higher-order modes are characterized by lower wavevectors (β) but with higher losses (κ) and an increasing number of oscillations in the lateral field distribution. The evanescent tail of the higher-order mode profiles extends more into the neighboring layers, making the mode more sensitive to the dielectric environment. Similar mode profiles can be obtained for the magnetic field in the case of TM polarization. In a realistic solar cell design including contact layers, the mode penetration outside the waveguide region needs to be accounted for to study the ratio of useful absorption in the waveguide mode compared to parasitic loss in the cladding materials [6, 7].

Figure 5(a) shows the dispersion curve for all TE modes (red) and TM modes (blue), indicating how the in-plane wavevector β changes as a function of free-space wavevector k_0. The black dashed line represents the light line in air. Figure 5(a) shows that all modes are dispersive as a result of dispersion in the c-Si waveguide core material. All dispersion curves are located below the light line, indicating that the modes are purely bound and cannot couple to far-field radiation. Light can only couple to the waveguide modes when mode overlap (governed by the polarization and mode profiles) and momentum matching are both fulfilled. The dispersion curves show how much in-plane momentum is needed to couple to the waveguide modes. One method for overcoming this momentum mismatch is to use a two-dimensional particle array which functions as a grating. For momentum matching to occur, the in-plane momentum of the waveguide mode has to be matched by the in-plane momentum of the incoming light plus the momentum generated by the grating.

To demonstrate experimentally that metal nanoparticle arrays can efficiently couple light to waveguide modes, we fabricate two-dimensional Ag nanoparticle arrays, with different particle diameters and array pitch, on top of an SOI wafer with similar structure as shown in the inset of figure 5(a).

The enhanced absorption in the 200 nm c-Si waveguide due to coupling to guided optical modes is measured optically
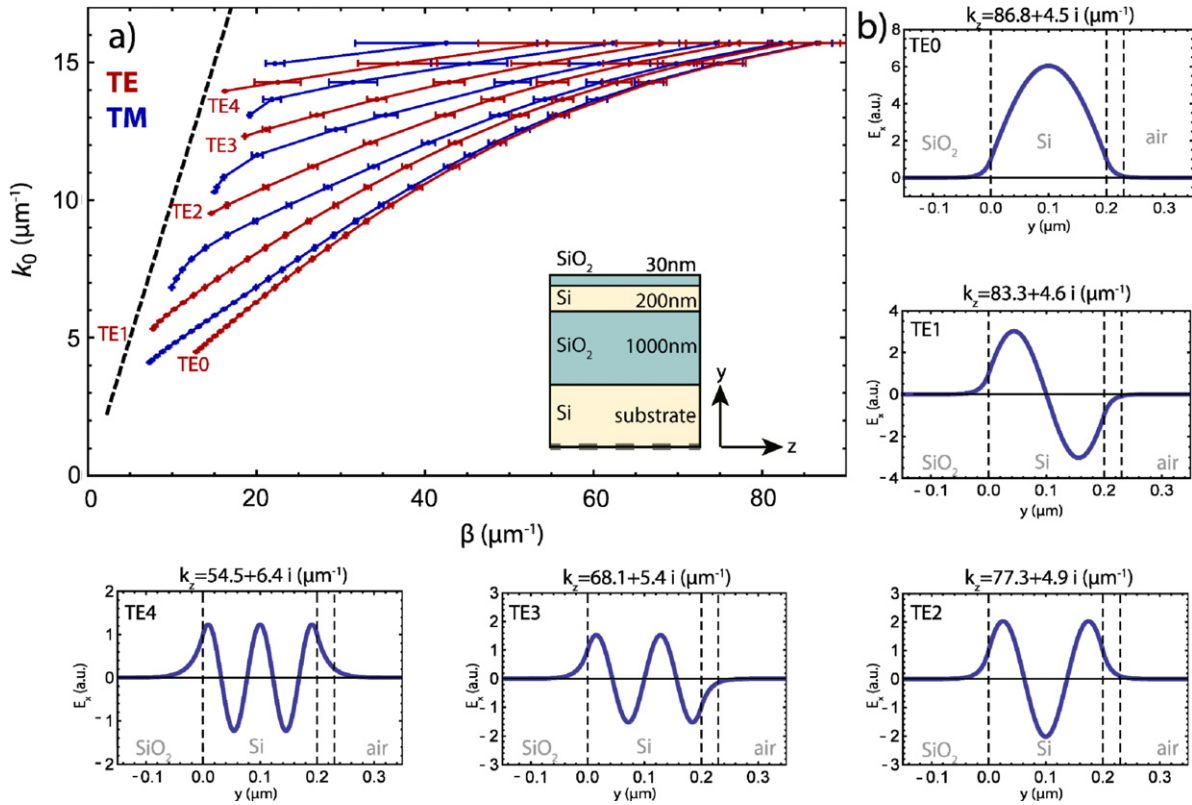
Figure 5. (a) Dispersion curve for the modes supported by the structure for 400 nm $< \lambda <$ 1500 nm. Red corresponds to TE modes and blue to TM modes. The dashed black line represents the light line in air. The inset is a schematic of the multilayer waveguide consisting of an SOI wafer with an SiO_2 spacer layer on top. The top silicon layer acts as a waveguide. The layer is assumed to be infinite in the two in-plane directions. (b) The five different TE modes supported by the waveguide $\lambda = 400$ nm. The complex parallel wavevector is also given for each mode. The vertical dashed lines depicted are the interfaces between the different layers.
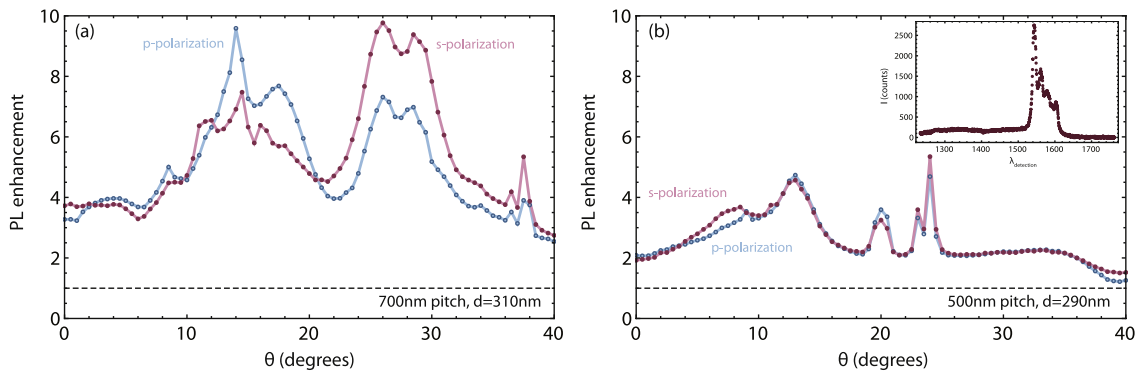

Figure 6. PL enhancement as a function of angle of incidence for a 700 nm pitched field (a) and a 500 nm pitched field (b). The blue lines (open symbols) correspond to p-polarized light and the red lines (solid symbols) to s-polarized light. Clear peaks are observed for both fields that are assigned to well-defined waveguide modes. A typical PL spectrum obtained from a non-patterned sample is shown as an inset, where the small peaks in the right shoulder are due to transitions between the Stark split energy levels of the $^4I_{13/2} \rightarrow ^4 I_{15/2}$ intra-4f transition of Er^{3+}. The peak of this spectrum is a direct probe of the intensity inside the waveguide.

by detecting the photoluminescence (PL) of Er ions implanted inside the waveguide [30]. 281 keV Er^+ (1×10^{15} cm^{-2}) and 40 keV O^+ (1×10^{16} cm^{-2}) were implanted and annealed at 680 °C for 30 min in an N_2 environment [31]. A typical PL spectrum for a non-patterned reference sample at $T = 14$ K when pumped with $\lambda = 980$ nm is shown in the inset of figure 6(b). The PL spectra of Er peaks at $\lambda = 1.54$ μm, a spectral region where c-Si is transparent. The small peaks in the right shoulder are due to transitions between the Stark split

energy levels of the $^4I_{13/2} \rightarrow ^4 I_{15/2}$ intra-4f transition of Er^{3+}. The peak of the signal at $\lambda = 1.54$ μm is used as a measure for the light intensity inside the waveguide, providing an optical probe of the 980 nm light trapping within the c-Si region. To probe the coupling to waveguide modes, the wavelength of the pump beam is fixed at $\lambda = 980$ nm and the angle of incidence is changed between 0° and 40°. Figure 6(a) shows the PL enhancement, defined as the PL signal of patterned

fields divided by the PL signal of non-patterned fields for p-polarized light (blue, open symbols) and s-polarized light (red, solid symbols) for a 700 nm pitch two-dimensional grating.

Clear peaks in the PL enhancement as a function of angle of incidence are observed. We attribute these peaks to light coupling into well-defined waveguide modes. The data show that coupling to waveguide modes enhances PL from the Er in the c-Si layer up to nearly a factor of 10 with respect to the emission from a non-patterned sample. The results of the 500 nm pitched fields, as shown in figure 6(b), show peaks at different angles than for the 700 nm pitch sample due to the different momentum generated by the grating.

By directly probing the intensity enhancement inside a c-Si waveguide we have shown that plasmonic particle arrays placed on top of a thin-film solar cell can provide an efficient light trapping scheme. Light coupling to waveguide modes can also be achieved, through the same momentum-matching mechanism, by a patterned metallic film on the back surface of the solar cell. In section 4, this scheme is used to integrate plasmonic particles in complete photovoltaic devices which improve the photocurrent and overall efficiency of a-Si:H thin-film solar cells.

4. Light trapping in thin-film a-Si:H solar cells

Light trapping has been a critical component of commercial thin-film Si solar cell design for decades, with most of the focus on the use of randomly textured surfaces [32]. For stability and manufacturability of a-Si:H solar cells, the active layers must be kept thin, even less than optically thick [33]. To achieve reasonable efficiencies with restricted device layer thicknesses, light trapping surfaces must be used to increase absorption within the semiconductor. Texture may be incorporated in both superstrate- and substrate-type depositions through the use of roughened plastics, textured transparent conducting oxides or hot, sputtered metal [34–39]. While these types of surfaces have received significant study, further improvements in cost and performance are necessary to make a-Si:H solar cells competitive with other available technologies. An important challenge for plasmonic integration in a-Si:H solar cells is to prove that there are advantages beyond those achievable with standard light trapping methods.

One approach to reducing the cost of a-Si:H solar cells is to reduce the thickness of the intrinsic layer: this both decreases the cost of feedstock material and increases the throughput rate of production, and can also increase the open-circuit voltage due to the decreased dark current in thin volumes [40, 41]. In these ultrathin-film geometries, coupling to waveguide modes is particularly important to decouple the direction of absorption from the direction of carrier collection.

For integration with full devices, we have focused on methods for inexpensive, scalable patterning of nanostructures. For any nanostructured technology to be effective in large-scale photovoltaics, it must be capable of patterning over large areas with good fidelity at low cost. We have used substrate conformal imprint lithography (SCIL), a novel form of nano-imprint lithography, which forms patterns by mechanical deformation of a resist material and is capable of printing

nanoscale features over wafer-scale areas [42]. Both the stamps used for imprinting and the master substrate for initial fabrication are reusable thousands of times. Nano-imprint lithography has also been used to replicate and transfer random textures from one transparent conducting oxide to another for photovoltaic applications [43].

In the work reviewed here, we used SCIL to pattern a 10×4 cm^2 area on a glass substrate with a variety of different periodic nanopatterns, allowing for a single solar cell deposition to test the light trapping properties of multiple patterned arrays. While many different processes may be used to fabricate a master template, we have specifically used interference lithography and electron-beam lithography to pattern c-Si master template wafers over large areas [44, 45]. SCIL is used to emboss a silica sol–gel resist on glass, then overcoated with Ag via sputtering to form the metallic back substrate and growth template for n–i–p a-Si:H solar cell deposition.

We have recently designed a back-contact light trapping surface for a-Si:H solar cells which show enhanced efficiency over cells with a commonly used random texture [45]. A schematic of the cell layout is shown in figure 7(a), along with the boundary conditions used for electromagnetic simulation of the response of the patterned solar cell. We pattern the metallic Ag back contact of the cell with an array of nanoparticles, then deposit the other layers conformally over the top of the Ag nanoparticle array. The light with wavelengths on the blue side of the spectrum is absorbed in the a-Si:H before reaching the back contact, while the red light that is more weakly absorbed scatters from the Ag nanoparticles and couples into the waveguide modes of the cell. Figure 7(b) shows an SEM image of one of the metallic nanoparticle arrays formed by Ag coating the imprinted silica sol–gel. The Ag patterns are then overcoated by ZnO:Al (which serves as a diffusion-blocking layer), n–i–p a-Si:H with 115 nm i-layer thickness, and 80 nm of ITO (which also serves as an AR coating). Each of the layers deposits conformally over the patterned arrays and a cross section of a fully fabricated device is shown in figure 7(c). The i-layer thickness used here is thinner than standard cells (115 nm versus 250 nm), and it is clear from the cross section that the active region is a small component of the total device thickness.

We tested several different pitches of square periodic arrays and figure 7(d) shows the measured J–V response of the best cells of each type. The cell area on which the J–V curves were measured is 0.13 cm^2, defined as the area of the ITO contact (0.16 cm^2) minus the area of the finger contacts. As a reference, we simultaneously deposited a-Si:H cells over the top of Ag/ZnO:Al-coated Asahi U type glass. While there are many different types of random texture, this is a commercial standard that facilitates comparison to other surfaces and is a more relevant comparison than flat, untextured devices. The open-circuit voltages of each of the patterns is similar, but there is a large difference in the short-circuit current density, as expected for cells with different light trapping efficiencies. Notably, the nanoparticles with a 500 nm pitch show 50% higher J_{sc} than the flat cells, and 10% higher than the randomly textured Asahi cells. The periodic array with 700 nm pitch
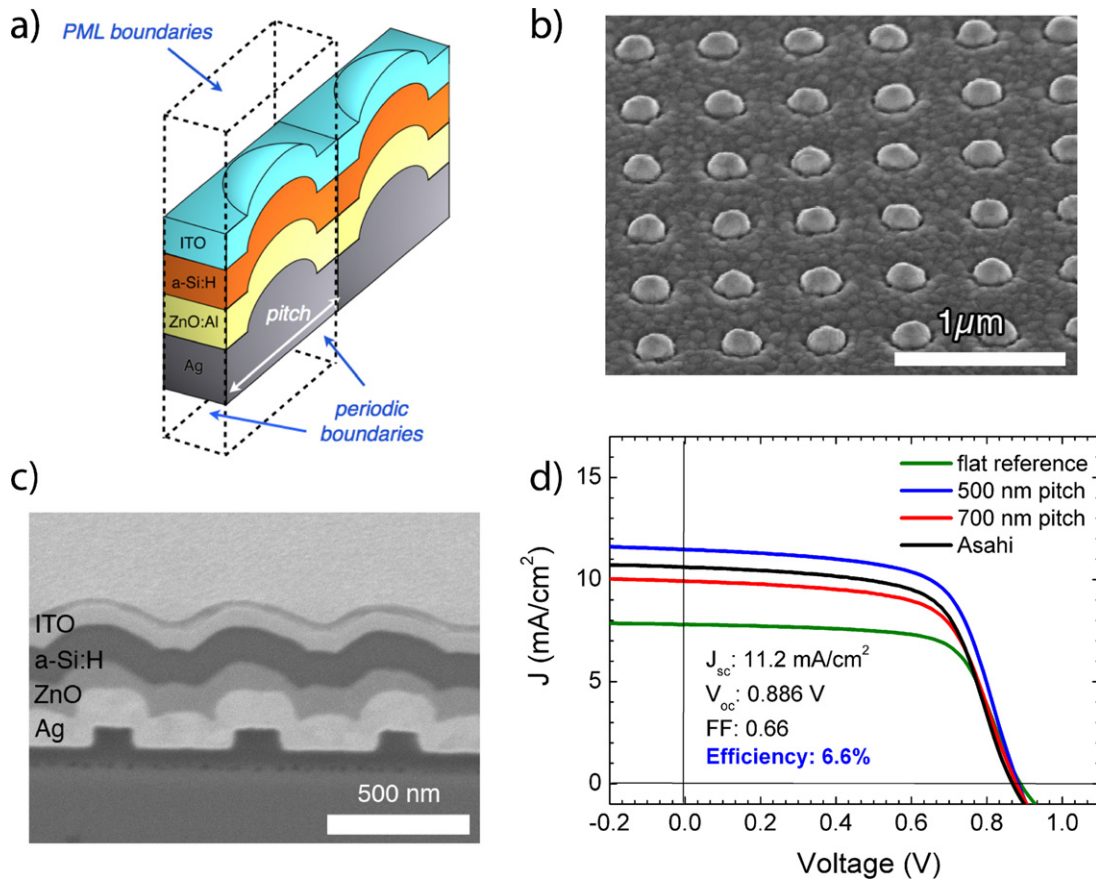
Figure 7. (a) Schematic of the cell layout, together with boundary conditions used in the FDTD simulations. (b) SEM image of a periodic array of Ag-coated sol–gel particles. (c) SEM image of an FIB cross section of a full nip type a-Si:H solar cell grown on the patterned back contact. (d) $J-V$ measurements of cells grown on different back patterns; inset shows the cell characteristics for the best cell, which is grown on top of a particle array with 500 nm pitch. Figures reproduced with permission: ©OSA (2011).
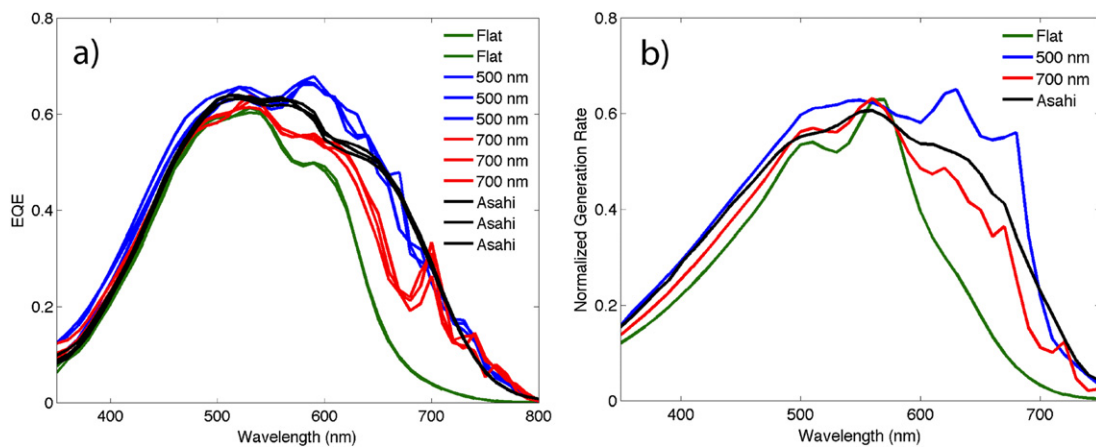

Figure 8. (a) EQE measurements on a-Si:H cells grown on top of different types of back reflectors. The multiple traces of each color represent the same type of back reflector in different measured devices, indicating the reproducibility. (b) Normalized generation rate calculated using FDTD simulations, showing good agreement with the experimentally determined photocurrent. Figures reproduced with permission: ©OSA (2011).

has slightly lower J_{sc} than the Asahi cell. Note that the PL measurements on c-Si waveguides showed better performance for the 700 nm pitch instead of the 500 nm pitch as for the a-Si solar cells. This is a result of the sensitivity of the optimum pitch to the layer thicknesses and geometry, such that the optimum pitch is specific to each case.

To look into the nature of this enhancement in more detail, we measured the external quantum efficiency (EQE) of the cells containing different patterns (figure 8(a)). The multiple traces of each color in the figure represent different measured devices, indicating the error margins on the photocurrent as well as the repeatability of the SCIL technique. Both the flat
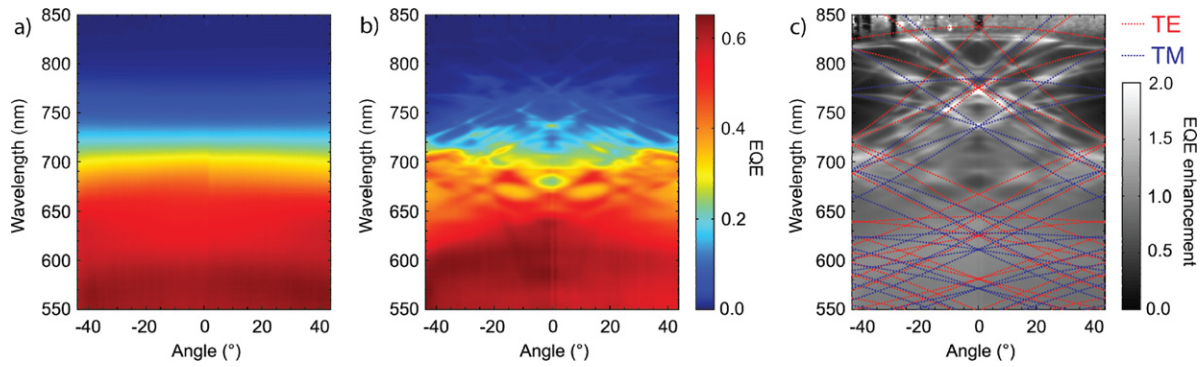
Figure 9. Angle-resolved photocurrent maps of Asahi (a) and 500 nm pitch periodic cells (b). The background of (c) shows the photocurrent enhancement of the periodic cell over the Asahi cell and the overlaid lines are the calculated waveguide modes in this structure. Figures reproduced with permission: ©OSA (2011).

and Asahi patterns have a very smooth response, while the 500 and 700 nm pitch periodic array cells show a number of sharp features in the EQE spectrum that are consistent across multiple devices. We attribute the presence of these peaks to the coupling to waveguide modes in the a-Si:H layer, defined by the periodicity of the pattern, as discussed in the section above. The 500 nm pitch cells show higher photocurrent than the randomly textured Asahi cells, particularly in the wavelength range from 550 to 650 nm.

We used optical electromagnetic simulation to verify the effects of light trapping and directly calculate the absorption in each layer of the solar cell. We used FDTD to explicitly calculate and isolate the generation rate (G_{opt}) in the a-Si:H region, according to

$$G_{opt} = \frac{1}{2\hbar}\varepsilon''|E|^2$$

where ε'' is the imaginary part of the permittivity and E is the electric field [7, 39]. This is an optical simulation only, which does not account for the role of carrier collection but is a reasonable approximation for understanding the absorption in the cell. Figure 8(b) shows the calculated generation rate from FDTD simulations on approximations of the fabricated pattern designs. The periodic patterns are simulated using a layout similar to the one shown in figure 7(a) with periodic boundary conditions accounting for the array. The Asahi patterns are simulated using directly imported AFM data. The correspondence between the measured and simulated photocurrent indicate that the effects are likely due to optical light trapping rather than to differences in the p-layer deposition over different types of patterns, or other growth and collection effects. The ability to simulate arbitrary textures (such as the Asahi cells) with good comparison to experimental cells makes FDTD a powerful design tool for nanostructured photovoltaics, both in terms of optimization and for physical understanding of the absorption mechanisms.

While we hypothesize that the peaks in the EQE spectra are due to waveguide modes, we can confirm the coupling using angle-resolved photocurrent spectroscopy [45]. Figure 9 shows angle-resolved maps of the photocurrent on the Asahi (figure 9(a)) and 500 nm pitch periodic (figure 9(b)) cells. If the peaks are due to waveguide modes, then the photocurrent

should shift with a changing angle of incidence. The Asahi cell is isotropic with respect to angle of incidence, while the periodic cell shows several crossings which sharpen with increasing wavelength where the absorption in the a-Si:H is weaker at longer wavelengths and the light propagates over more nanostructures. The background of figure 9(c) shows the photocurrent enhancement of the periodic cell over the Asahi cell and the overlaid lines are the calculated waveguide modes in this structure. The close agreement indicates that these features are due to waveguide modes and that waveguide modes do increase the photocurrent in a fully operational solar cell.

While these nanopatterns do not represent an optimum for light trapping in a-Si:H, they do show the promise of nanostructures designed for enhancing photocurrent in solar cells [46]. While a wide variety of randomly textured reference surfaces exist with different performances, designed nanostructures offer the advantage of precise control and understanding of light management in photovoltaics, and for guiding and directing light absorption at the nanoscale.

5. Conclusions

The application of surface plasmons to solar cells is an emerging field with the potential to improve the overall cost per watt of thin-film devices by reducing material usage: high-efficiency cells can be made using less material. For semiconductors based on scarce elements, which were not discussed in detail here, this may also alleviate some of the issues with raw material availability. For thin-film Si devices, the ability to reduce the overall thickness can even increase the efficiency, due to improved carrier collection, reduced bulk recombination and reduced photodegradation. Fabricating thinner cells leads to an increased manufacturing throughput, which reduces costs. The nano-imprint process, including the silver particle material, will add costs. Further studies are required to make a full estimate of the cost benefits of the plasmonic cell design.

Here we reviewed two different geometries for plasmonic integration with solar cells, placing nanoparticles either on the front surface of c-Si-based devices or on the back contact for a-Si:H-based devices. In section 2, we showed that

by integrating plasmonic nanostructures with AR coatings, a broadband reduction in reflectance can be achieved on bulk c-Si wafers. Such metal scattering layer can subsequently be used to cause enhanced light trapping into waveguide modes of the cell. In section 3, we used erbium-implanted SOI wafers as a model system to optically probe coupling to waveguide modes in ultrathin c-Si layers. From the PL intensity enhancement we derive that coupling to waveguide modes of the c-Si region leads to up to 10-fold enhanced light trapping. In section 5, we integrated plasmonic nanostructures with the back contact of an a-Si:H device and showed that coupling to waveguide modes increases the photocurrent and the overall efficiency of the cell over that of a particular reference randomly textured cell. Combined, these studies highlight a few of the possibilities for integrating plasmonics with photovoltaic devices and show that systematic study of particle geometries and arrangements can give insight on the way to optimum design.

The implementation of plasmonic solar cells as high-efficiency devices that can be manufactured at a competitive price is so far mainly limited by the fact that the field is still relatively new. One challenge is to integrate plasmonic nanostructures into existing device architectures. Several important challenges in this area have already been investigated, such as integration with antireflection coatings, integration into metallic back contacts and large-scale, inexpensive patterning. Another challenge is to achieve broadband and angle-isotropic photocurrent enhancement, such that the cells operate well over the course of the day. Nanostructure designs for higher-efficiency III–V and multijunction cells are another area for study.

Acknowledgments

References

[1] Green M A 1998 *Solar Cells: Operating Principles, Technology and System Applications* (Sydney: University of South Wales)

[2] Yablonovitch E 1982 Intensity enhancement in textured optical sheets for solar cells *IEEE Trans. Electron. Devices* **29** 300–5

[3] Yablonovitch E 1982 Statistical ray optics *J. Opt. Soc. Am.* **72** 899–907

[4] Atwater H A and Polman A 2010 Plasmonics for improved photovoltaic devices *Nature Mater.* **9** 205

[5] Catchpole K R and Polman A 2008 Plasmonic solar cells *Opt. Express* **16** 21793

[6] Saeta P N, Ferry V E, Pacifici D, Munday J N and Atwater H A 2009 How much can guided modes enhance absorption in thin solar cells? *Opt. Express* **17** 20975

[7] Ferry V E, Munday J N and Atwater H A 2010 Design considerations for plasmonic photovoltaics *Adv. Mater.* **22** 4794–808

[8] Catchpole K R and Polman A 2008 Design principles for particle plasmon enhanced solar cells *Appl. Phys. Lett.* **93** 191113

[9] Beck F J, Polman A and Catchpole K R 2009 Tunable light trapping for solar cells using localized surface plasmons *J. Appl. Phys.* **105** 114310

[10] Mokkapati S, Beck F J, Polman A and Catchpole K R 2009 Designing periodic arrays of metal nanoparticles for light-trapping applications in solar cells *Appl. Phys. Lett.* **95** 053115

[11] Stuart H R and Hall D G 1996 Absorption enhancement in silicon-on-insulator waveguides using metal island films *Appl. Phys. Lett.* **69** 2327

[12] Stuart H R and Hall D G 1998 Island size effects in nanoparticle-enhanced photodetectors *Appl. Phys. Lett.* **73** 3815

[13] Schaadt D M, Feng B and Yu E T 2005 Enhanced semiconductor optical absorption via surface plasmon excitation in metal nanoparticles *Appl. Phys. Lett.* **86** 63106

[14] Derkacs D, Lim S H, Matheu P, Mar W and Yu E T 2006 Improved performance of amorphous silicon solar cells via scattering from surface plasmon polaritons in nearby metallic nanoparticles *Appl. Phys. Lett.* **89** 93103

[15] Derkacs D, Chen W V, Matheu P M, Lim S H, Yu P K L and Yu E T 2008 Nanoparticle-induced light scattering for improved performance of quantum-well solar cells *Appl. Phys. Lett.* **93** 091107

[16] Pillai S, Catchpole K R, Trupke T and Green M A 2007 Surface plasmon enhanced silicon solar cells *J. Appl. Phys.* **101** 93105

[17] Nakayama K, Tanabe K and Atwater H 2008 Plasmonic nanoparticle enhanced light absorption in GaAs solar cells *Appl. Phys. Lett.* **93** 121904

[18] Spinelli P, Van Lare M, Verhagen E and Polman A 2011 Controlling Fano lineshapes in plasmon-mediated light coupling into a substrate *Opt. Express* **19** A303

[19] Spinelli P, Hebbink M, de Waele R, Black L, Lenzmann F and Polman A 2011 Optical impedance matching using coupled metal nanoparticle arrays *Nano Lett.* **11** 1760

[20] Hägglund C, Zäch M, Petersson G and Kasemo B 2008 Electromagnetic coupling of light into a silicon solar cell by nanodisk plasmons *Appl. Phys. Lett.* **92** 053110

[21] Kippenberg T J, Tchebotareva A L, Kalkman J, Polman A and Vahala K J 2009 Purcell factor enhanced scattering from Si nanocrystals in an optical microcavity *Phys. Rev. Lett.* **103** 027406

[22] Mertz J 2000 Radiative absorption, fluorescence, and scattering of a classical dipole near a lossless interface: a unified description *J. Opt. Soc. Am.* B **17** 1906–13

[23] Lim S H, Mar W, Matheu P, Derkacs D and Yu E T 2007 Photocurrent spectroscopy of optical absorption enhancement in silicon photodiodes via scattering from surface plasmon polaritons in gold nanoparticles *J. Appl. Phys.* **101** 104309

[24] Luk'yanchuk B, Zheludev N I, Maier S A, Halas N J, Nordlander P, Giessen H and Chong C T 2010 The Fano resonance in plasmonic nanostructures and metamaterials *Nature Mater.* **9** 707

[25] Lassiter J B, Sobhani H, Fan J A, Kundu J, Capasso F, Nordlander P and Halas N J 2010 Fano resonances in plasmonic nanoclusters: geometrical and chemical tunability *Nano Lett.* **10** 3184

[26] Xu G, Tazawa M, Jin P, Nakao S and Yoshimura K 2003 Wavelength tuning of surface plasmon resonance using dielectric layers *Appl. Phys. Lett.* **82** 3811

[27] Snyder A W and Love J D 1983 *Optical Waveguide Theory* (London: Chapman and Hall)

[28] Stuart H R and Hall D G 1998 Enhanced dipole–dipole interaction between radiators near a surface *Phys. Rev. Lett.* **80** 5663–6

[29] Verhagen E 2010 Subwavelength light confinement with surface plasmon polaritons *PhD Thesis* FOM Institute AMOLF www.amolf.nl

[30] Polman A 2001 Erbium as a probe of everything? *Physica* B **300** 78–90

[31] Polman A 1997 Erbium implanted thin film photonic materials *J. Appl. Phys.* **82** 1

[32] Schropp R E I and Zeman M 1998 *Amorphous and Microcrystalline Silicon Solar Cells: Modeling, Materials, and Device Technology* (Boston: Kluwer Academic)

[33] Deng X and Schiff E A 2003 *Handbook of Photovoltaic Science and Engineering: Amorphous Silicon-based Solar Cells* (New York: Wiley)

[34] Dagkaldiran U, Gordijn A, Finger F, Yates H M, Evans P, Sheel D W, Remes Z and Vanecek M 2009 Amorphous silicon solar cells made with SnO_2:F TCO films deposited by atmospheric pressure CVD *Mater. Sci. Eng.* B **159/60** (Sp. Iss. SI) 6–9

[35] Krc J, Smole F and Topic M 2003 Potential of light trapping in microcrystalline silicon solar cells with textured substrates *Prog. Photovolt.* **11** 429–36

[36] Franken R H, Stolk R L, Li H, van der Werf C H M, Rath J K and Schropp R E I 2007 Understanding light trapping by light scattering textured back electrodes in thin film n–i–p-type silicon solar cells *J. Appl. Phys.* **102** 014503

[37] Muller J, Rech B, Springer J and Vanecek M 2004 TCO and light trapping in silicon thin film solar cells *Sol. Energy* **77** 917–30

[38] Niira K, Senta H, Hakuma H, Komoda M, Okui H, Fukui K, Arimune H and Shirasawa K 2002 Thin film poly-Si solar cells using PECVD and Cat-CVD with light confinement structure by RIE *Sol. Energy Mater. Sol. Cells* **74** 247–53

[39] Fahr S, Rockstuhl C and Lederer F 2008 Engineering the randomness for enhanced absorption in solar cells *Appl. Phys. Lett.* **92** 171114

[40] Campbell P and Green M A 1986 The limiting efficiency of silicon solar-cells under concentrated sunlight *IEEE Trans. Electron Devices* **33** 234–9

[41] Fahrenbruch A L and Bube R H 1983 *Fundamentals of Solar Cells: Photovoltaic Solar Energy Conversion* (London: Academic)

[42] Verschuuren M and van Sprang H 2007 3D photonic structures by sol–gel imprint lithography *Material Research Society Symposium Proceedings* vol 1002, Materials Research Society (Cambridge, UK: Cambridge University Press) pp N03–05

[43] Battaglia C *et al* 2011 Nanoimprint lithography for high-efficiency thin-film silicon solar cells *Nano Lett.* **11** 661–5

[44] Ferry V E, Verschuuren M A, Li H B T, Schropp R E I, Atwater H A and Polman A 2009 Improved red-response in thin film a-Si:H solar cells with soft-imprinted plasmonic back reflectors *Appl. Phys. Lett.* **95** 183503

[45] Ferry V E, Verschuuren M A, Li H B T, Verhagen E, Walters R J, Schropp R E I, Atwater H A and Polman A 2010 Light trapping in ultrathin plasmonic solar cells *Opt. Express* **18** A237–45

[46] Ferry V E, Verschuuren M A, van Lare M, Schropp R E I, Atwater H A and Polman A 2011 Optimized spatial correlations for broadband light trapping nanopatterns in high efficiency ultra-thin film a-Si:H solar cells *Nano Lett.* at press